

One-loop decays $A^0 \rightarrow ZZ, Z\gamma, \gamma\gamma$ within the 2HDM and its search at the LHC

J. L. Diaz-Cruz^{*}

*Facultad de Ciencias Físico-Matemáticas,
Benemérita Universidad Autónoma de Puebla,
C.P. 72570, Puebla, Pue., Mexico. and
Departamento de Física, CINVESTAV,
Apdo. Postal 14-740, 07000 México, D. F., México.*

C. G. Honorato[†] and M. A. Pérez[‡]

*Departamento de Física, CINVESTAV,
Apdo. Postal 14-740, 07000 México, D. F., México.*

J. A. Orduz-Ducuara[§]

*Facultad de Ciencias Físico -Matemáticas
Benemérita Universidad Autónoma de Puebla, C.P. 72570, Puebla, Pue., Mexico.*

(Dated: March 3, 2022)

The general two-Higgs doublet model (2HDM) contains a rich spectrum of neutral and charged Higgs bosons, whose detection would be a clear signal of new physics. When the Higgs potential is CP conserving, the spectrum includes a pseudoscalar mass eigenstate A^0 , which does not couple to vector bosons at tree level. However, fermionic loops (top and bottom mainly) induce the coupling AVV' (with $V, V' = \gamma, Z$) at higher orders. We evaluate the amplitude for the decays $A^0 \rightarrow ZZ, Z\gamma, \gamma\gamma$, including a generic fermionic loop contribution, and present results on the branching ratios for 2HDM-I,II and III. Current LHC searches on heavy Higgs bosons are used as an estimate to constrain the allowed mass range for A^0 .

PACS numbers: 14.80.Ec, 14.70.-e

^{*} jldiaz@cfm.buap.mx

[†] carlos_honorato@ymail.com

[‡] mperez@fis.cinvestav.mx

[§] jaorduz@gmail.com

I. INTRODUCTION

After many years of planning and preparation, the LHC has found evidence of a Higgs-like particle, with mass $m_h = 125 \sim 126 \text{ GeV}$ [1, 2]. It is remarkable that the observed Higgs mass falls within the range preferred by the analysis of electroweak precision tests, within the Standard Model [3]. Although the measured couplings point towards a SM Higgs interpretation for such particle, more data will be needed in order to determine whether this resonance belongs to the SM or to some of its extensions; in the later case its properties could deviate from the SM expectations [4].

On the other hand, the LHC has also searched for signals of new physics beyond the SM, either through the production of new particles or by looking for anomalous couplings for the SM particles [5]. However, so far current LHC studies have not detected any evidence of new physics, and the resulting bounds on the associated scale has been pushed into the TeV territory [6]. In fact, the weakest bounds are precisely on the search for heavy Higgs particles [7–9], which are predicted in many models of new physics, including SUSY, XD, GUTs etc [10–13]. Thus, searching for those Higgs particles could provide the first signal on physics beyond the SM. Furthermore, this task could be attempted now with some degree of optimism, because once the LHC has detected a scalarlike state, it seems possible that more scalars could appear in the future LHC data.

One of the simplest extensions of the SM consists of the addition of an extra Higgs doublet, the so-called two-Higgs doublet model (2HDM), which has been widely studied in all the presentations that have been proposed (2HDM I, II, III, X, Y, etc) [14]. Some interesting properties of the 2HDM include

- A rich Higgs boson spectrum is predicted within this model, which includes three neutral degrees of freedom and one charged Higgs boson (H^\pm),
- Among the neutral states, the model predicts the existence of a pseudoscalar state A^0 , which would be a clear sign of new physics, and whose phenomenology we are interested in.
- When the Higgs potential is CP conserving, A^0 is also a mass eigenstate [15]
- Because of the quantum number assignments and discrete symmetries of the model,

this state does not couple to vector bosons at tree level. However, such couplings could be induced at loop level [16, 17].¹

In this paper, we are interested in studying the one-loop decays of the pseudoscalar A into a pair of vector bosons, namely $A^0 \rightarrow ZZ, Z\gamma, \gamma\gamma$, within the context of the two-Higgs doublet model (2HDM), some of these decays have been studied in effective Lagrangian context [18, 19]. We shall work within the versions of the model where the Higgs sector respects CP symmetry, which could occur in 2HDM-I, II and III; in this case A^0 is actually a mass eigenstate. The loop amplitude for $A \rightarrow VV'$ receives contributions from heavy fermions, mainly from the top and bottom quarks.

It turns out that the fermionic contribution within 2HDM I, II, depends only on the Yukawa Lagrangian parameters, which reduce in the end to $\tan\beta$ (the ratio of the vacuum expectation values, i.e. $\tan\beta = v_2/v_1$) and the fermion masses. On the other hand, within the 2HDM-III, where one assumes some texture structure for the Yukawa matrices [20], one needs to consider additional parameters, which are called χ_{ij} [21]. For $i \neq j$ those couplings would induce flavor-changing neutral currents (FCNC) mediated by the scalars, while for $i = j$ those couplings would correct the usual 2HDM predictions for the diagonal Higgs-fermion couplings [22]. The dominant contribution to the loop amplitude in the low and moderate $\tan\beta$ ($\simeq 1 - 5$) comes from the top quark. For larger values of $\tan\beta$, which seem disfavored by low energy constraints on the 2HDM, the bottom quark contribution should also be included.

The organization of this paper goes as follows. Section II contains a discussion of the general 2HDM and its limiting cases, focusing on the Higgs-fermion couplings. Section III includes a discussion of the decay amplitude for the process $A \rightarrow VV'$, written in general terms, i.e. including the most general couplings of the pseudoscalar A^0 with fermions; we also present the simplified expressions for the decay widths of the decays $A^0 \rightarrow ZZ, Z\gamma, \gamma\gamma$. Then, in Sec. IV we discuss the numerical results for the branching ratios, and we identify regions of parameters where those decays show a large branching ratio. Then, we study the constraints that current searches for heavy Higgs bosons at the LHC could impose on the parameters of the model. This is done through the evaluation of the signal strengths (R_{ZZ}), which are used as an estimate for the signal coming from $A^0 \rightarrow ZZ$. Our conclusions are

¹ Besides presenting a numerical study of these loop-induced decays, Ref. [17] also presents an analysis of the reaction $pp \rightarrow VV$, but before data on 126 GeV Higgs were presented by the LHC.

left for Sec. V.

II. THE TWO-HIGGS DOUBLET MODEL (2HDM)

In order to specify the 2HDM versions, of types I , II and III, one needs to define the Yukawa sector, which includes the interactions of the Higgs doublets with the quarks and leptons. Interactions with gauge bosons come from the covariant derivatives, and the pattern of spontaneous symmetry breaking is associated with the Higgs potential [23]. The general 2HDM-III is defined by the Yukawa Lagrangian [24]

$$\mathcal{L} = Y_1^u \overline{Q}_L^0 \tilde{\Phi}_1 u_R^0 + Y_2^u \overline{Q}_L^0 \tilde{\Phi}_2 u_R^0 + Y_1^d \overline{Q}_L^0 \Phi_1 d_R^0 + Y_2^d \overline{Q}_L^0 \Phi_2 d_R^0 + h.c. \quad (1)$$

where

$$Q_L^0 = \begin{pmatrix} u_L \\ d_L \end{pmatrix}, \quad \overline{Q}_L^0 = (\overline{u}_L, \overline{d}_L), \quad \Phi_1 = \begin{pmatrix} \phi_1^\pm \\ \phi_1 \end{pmatrix}, \quad \Phi_2 = \begin{pmatrix} \phi_2^\pm \\ \phi_2 \end{pmatrix}, \quad \tilde{\Phi}_j = i\sigma_2 \Phi_j^* = \begin{pmatrix} \phi_j^* \\ -\phi_j^\mp \end{pmatrix} \quad (2)$$

and $\phi_i = \frac{1}{\sqrt{2}}(v_i + \phi_i^0 + i\chi_i)$.

For the purposes of this paper, it suffices to consider the case when the Higgs sector is CP conserving, then the CP-even Higgs states (h and H) come from the mixing of the real parts of the neutral components, ϕ_1^0 and ϕ_2^0 , while one combination of the imaginary components, χ_1^0 and χ_2^0 , give place to the pseudo-Goldstone boson (needed to give mass to the Z boson), while the corresponding orthogonal combination denotes the CP-odd state A^0 . The mixing angles α and β that appear in the neutral Higgs mixing, corresponds to the standard notation, i.e. $\tan \beta = v_2/v_1$.

Then, the interactions of the pseudoscalar Higgs boson (A^0) with the up-type quarks, are given by the following Lagrangian [25]:

$$\mathcal{L}_{up}^{neutral} = \overline{u}_i (S_{ijA}^u + i\gamma^5 P_{ijA}^u) u_j A^0 + h.c. \quad (3)$$

with

$$S_{ijA}^u = i \frac{\sqrt{m_i m_j}}{2\sqrt{2}v \cos \beta} (\chi_{ij} - \chi_{ij}^\dagger), \quad (4)$$

$$P_{ijA}^u = \frac{1}{2v} M_{ij}^U \cot \beta - \frac{\sqrt{m_i m_j}}{2\sqrt{2}v \sin \beta} (\chi_{ij} + \chi_{ij}^\dagger) \quad (5)$$

Similar equations hold for d-type quarks and leptons (see [25]).

As discussed in Ref. [24], the assumption of universal textures for the Yukawa matrices, allows to express one Yukawa matrix, for instance Y_2^f , in terms of the quark masses, and parametrize the flavor changing neutral scalar interactions (FCNSI) in terms of the unknown coefficients χ_{ij} , which appear in the other Yukawa matrix, written in the mass-eigenstates basis, namely $\tilde{Y}_{2ij}^U = \chi_{ij} \frac{\sqrt{m_i m_j}}{v}$, although other combinations are possible, for instance the complementary textures discussed in Ref. [26]. These parameters can be constrained by considering all types of low energy FCNC transitions; and although these constraints are quite strong for transitions involving the first and second families, as well as for the b-quark, it turns out that they are rather mild for the top quark [27, 28].

Furthermore, we only need to look at the diagonal couplings of A^0 to up-, down-type quarks and charged leptons, denoted generically as f_i , because of their contribution to the loop amplitudes. Thus, the relevant Lagrangian can be written as

$$\mathcal{L}_{A^0}^f = \frac{gm_i^f}{2m_W} \bar{f}_i \left(g_{Si}^f + i\gamma^5 g_{Pi}^f \right) f_i A^0. \quad (6)$$

When the Yukawa matrices are taken to be Hermitian, only the pseudoscalar coupling remains; i.e., $g_{Si}^f = 0$, and one finds for the diagonal coupling,

$$g_{Pi}^u = \cot \beta - \frac{1}{\sin \beta} (\chi_{ii}), \quad (7)$$

where the χ_{ii} can be taken essentially as free parameters.

For 2HDM I and II, the χ vanish, and thus only the pseudoscalar part contribute. Table I shows the vertex $A^0 f \bar{f}$ for $f = u, d$ type-quarks, within the CP-conserving case.

TABLE I. The vertex $A^0 uu$ and $A^0 dd$ for 2HDM-I-II and III type [14].

	Type I	Type II	Type III
g_P^u	$\cot \beta$	$\cot \beta$	$\cot \beta - \frac{1}{\sin \beta} (\chi_{ii}^u)$
g_P^d	$-\cot \beta$	$\tan \beta$	$\tan \beta - \frac{1}{\cos \beta} (\chi_{ii}^d)$
g_P^l	$-\cot \beta$	$\tan \beta$	$\tan \beta - \frac{1}{\cos \beta} (\chi_{ii}^l)$

III. THE GENERAL EXPRESSIONS FOR THE AMPLITUDES AND DECAY WIDTHS FOR $A \rightarrow VV'$

In this section we shall present the calculation of the one-loop amplitude for the decay $A \rightarrow VV'$, where V, V' represent any neutral SM vector boson ($V, V' = \{\gamma, Z\}$). Due to the parity properties of the pseudoscalar, the vertex AVV' , as well as AW^+W^- , are not present at tree level, when the Higgs sector is CP conserving. However, this vertex could be induced at one the loop-level from different sources. But in a model where the Higgs potential is CP conserving, the coupling between A^0 and H^+H^- is also forbidden, and thus the charged Higgs does not contribute to the loop-induced vertex AVV' . While in other models, such as the MSSM, there are plenty of other particles that could contribute to the AVV' vertex, here we shall focus on the fermionic contributions only. This choice is made because of our goal to perform a numerical analysis based on a few free parameters, as well as the recent limits on the masses of new particles, beyond the SM, which are reaching the TeV range, whose contributions to the vertex AVV' are likely to be highly suppressed. The Feynman diagrams for the amplitude are shown in Fig. 1. We shall consider the most general $A^0 f \bar{f}$ couplings, i.e. allowing for the possibility of having a new source of CP violating associated with the non-Hermiticity of the Yukawa matrices.² Then we shall present specific formulas for the decay widths within the 2HDM I, II and general III-type.

A. The decay amplitudes for $A \rightarrow VV'$

Thus, the amplitude for the process $A \rightarrow VV'$, will be written in general, namely we shall consider in equation (6). The fermion-gauge vertices are written as: $g_{Vff} = -ik_{Vff}\gamma_\mu(g_v^f - g_a^f\gamma^5)$, then for $V = Z$ we have $k_{Zff} = \frac{g}{4\cos\theta_W}$ and for $V = \gamma$, $k_{\gamma ff} = e|Q_f|$, $g_v^f = 1$, $g_a^f = 0$.

The kinematics conditions are defined according to the following configuration of momentum: $p_3 = p_1 + p_2$. Then according to Fig. 1, we have that: $p_3^2 = m_A^2$, $p_1^2 = m_{V'}^2$, $p_2^2 = m_V^2$ and $2p_1 \cdot p_2 = m_A^2 - m_{V'}^2 - m_V^2$.

The general tensorial amplitude for AVV' vertex is written as follows,

$$\mathcal{M}^{\mu_1\mu_2} = \frac{ig r_f N_C k_{V_1ff} k_{V_2ff}}{16m_W\pi^2(1 - 2(r_1 + r_2) + (r_1 - r_2)^2)^2} \mathcal{A}_{VV'}^{\mu_1\mu_2} \epsilon_{\mu_1}^* \epsilon_{\mu_2}^*, \quad (8)$$

² The numerical analysis for the case with CPV in the Higgs potential, and its comparison with CPV from the Yukawa sector will be presented in a future publication.

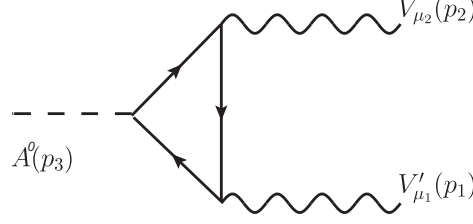


FIG. 1. Feynman diagram for $A \rightarrow VV'$ decay, only fermion particles are present. Crossed diagram is not shown.

where $r_i = \frac{M_{V_i}^2}{m_A^2}$, and

$$\mathcal{A}_{VV'}^{\mu_1\mu_2} = g_S^f \left(\mathcal{A}_1 g^{\mu_1\mu_2} + \mathcal{A}_2 p_2^{\mu_1} p_1^{\mu_2} \right) + g_P^f \mathcal{A}_3 \epsilon^{\alpha\beta\mu_1\mu_2} p_{1\alpha} p_{2\beta}. \quad (9)$$

Here one can see how the $A^0 f \bar{f}$ couplings give place to different tensorial structures, with the pseudoscalar part (i.e. g_{Pi}^f) inducing the term proportional to the Levi-Civita tensor, as expected. The corresponding form factors are given by

$$\begin{aligned} \mathcal{A}_1 = & g_{v_1}^f g_{v_2}^f m_A^2 (r_1^2 - 2(r_2 + 1)r_1 + (r_2 - 1)^2) \times \\ & \left(\left\{ \frac{m_A^2}{2} (4r_f + 2r_1(r_1(4r_f - r_2 - 3) - 4(r_2 + 2)r_f + r_1^2 + r_2 + 3) - 1) C_0(V_1, V_2) \right. \right. \\ & \left. \left. + 2r_1(1 - r_1 + r_2) \Delta B_0(A, V_1) + 2r_1^2 - 2(r_2 + 2)r_1 + 1 \right\} + \left\{ 1 \leftrightarrow 2 \right\} \right) \\ & + g_{a_1}^f g_{a_2}^f m_A^2 (r_1^2 - 2(r_2 + 1)r_1 + (r_2 - 1)^2) \times \\ & \left(\left\{ \frac{m_A^2}{2} (2r_1^2(-4r_f - r_2 - 1) + 2r_1(8r_f + r_2(4r_f - 1) - 1) - 4r_f + 2r_1^3 + 1) C_0(V_1, V_2) \right. \right. \\ & \left. \left. + 2(2r_2r_1 - r_1^2 - r_2^2 + 2r_1 + 2r_2 - 1) B_0^R + 2(r_2^2 - r_1r_2 - 2r_2 - r_1 + 1) \Delta B_0(A, V_1) \right. \right. \\ & \left. \left. + 2r_1^2 - 2(r_2 + 2)r_1 + 1 \right\} + \left\{ 1 \leftrightarrow 2 \right\} \right), \end{aligned}$$

$$\begin{aligned}
\mathcal{A}_2 = & g_{v_1}^f g_{v_2}^f \left(\left\{ m_A^2 (r_1 + r_2 - 1) C_0(V_1, V_2) \times \right. \right. \\
& \left(2r_1^2 (4r_f - r_2 - 3) - 2r_1 (8r_f + r_2 (4r_f - 5) - 3) + 4r_f + 2r_1^3 - 1 \right) \\
& + 4 \left(r_1^3 + 4r_2 r_1^2 - 2r_1^2 - 5r_2^2 r_1 + 4r_2 r_1 - (r_1^2 - (r_2 + 2)r_1 + 2r_2 + 1)r_1 + r_1 \right) B_0^R(A) \\
& + 4(-r_1^3 - 4r_2 r_1^2 + 2r_1^2 + 5r_2^2 r_1 - 4r_2 r_1 - r_1) \Delta B_0(A, V_1) \\
& \left. + 4r_1 (r_1^2 - (r_2 + 3)r_1 - r_2 + 3) - 2 \right\} + \left\{ 1 \leftrightarrow 2 \right\} \Bigg) \\
& + (r_1 + r_2 - 1) g_{a_1}^f g_{a_2}^f \times \\
& \left(\left\{ m_A^2 \left(4r_f + 2r_1 (r_1 (4r_f - r_2 - 1) - 4(r_2 + 2)r_f + r_1^2 + 3r_2 - 1) + 1 \right) C_0(V_1, V_2) \right. \right. \\
& + 4 \left(r_1^2 - 2r_1 - r_2^2 + 2r_2 \right) B_0^R + 4((r_2 - 1)^2 + (r_2 + 1)r_1 - 2r_1^2) \Delta B_0(A, V_1) \\
& \left. \left. + 4r_1^2 - 4(r_2 + 2)r_1 + 2 \right\} + \left\{ 1 \leftrightarrow 2 \right\} \right),
\end{aligned}$$

and

$$\begin{aligned}
\mathcal{A}_3 = & -m_A^2 g_{v_1}^f g_{v_2}^f \left(\left\{ 2r_1^4 - 8(r_2 + 1)r_1^3 + 2(3r_2^2 + 4r_2 + 6)r_1^2 + 4(r_2 - 2)r_1 + 1 \right\} + \left\{ 1 \leftrightarrow 2 \right\} \right) C_0(V_1, V_2) \\
& - g_{a_1}^f g_{a_2}^f (r_1^2 - 2(r_2 + 1)r_1 + (r_2 - 1)^2) \times \\
& \left(\left\{ m_A^2 (2r_1^2 - 2r_2 r_1 - 1) C_0(V_1, V_2) - 4(r_1 - r_2 + 1) \Delta B_0(A, V_1) \right\} + \left\{ 1 \leftrightarrow 2 \right\} \right),
\end{aligned}$$

where $B_0(i) = B_0(m_i^2, m_f^2, m_f^2)$, $\Delta B_0(i, j) = B_0(i) - B_0(j)$, $C_0(i, j) = C_0(m_A^2, m_i^2, m_j^2, m_f^2, m_f^2, m_f^2)$.

We have used the renormalization method described in [29], which allows us to write:

$B_0^R = B_0(m_A^2, m_f^2 + \mu_R^2, m_f^2 + \mu_R^2) - B_0(0, \mu_R^2, \mu_R^2)$, where μ_R denotes a renormalization scale.

These expressions show the Bose symmetry explicitly.

B. The decay widths for $A^0 \rightarrow ZZ, Z\gamma, \gamma\gamma$

In this section we shall present the expressions for the decay widths corresponding to the processes: $A^0 \rightarrow ZZ, Z\gamma, \gamma\gamma$, which follow from the above expressions for the amplitudes.

1. The expression for the decay width for $A^0 \rightarrow ZZ$ is

$$\Gamma(A^0 \rightarrow ZZ) = m_A \frac{\kappa_{ZZ} r_f}{(1 - 4r_Z)^{1/2}} \left(\frac{g_S^{f^2}}{(1 - 4r_Z)^3} \left(g_a^{f^4} \mathcal{G}_a^{ZZ} + 2g_v^{f^2} g_a^{f^2} \mathcal{G}_{av}^{ZZ} + g_v^{f^4} \mathcal{G}_v^{ZZ} \right) + \frac{g_P^{f^2}}{2} \left(g_a^{f^2} \mathcal{F}_a^{ZZ} - g_v^{f^2} \mathcal{F}_v^{ZZ} \right)^2 \right), \quad (10)$$

where $\kappa_{ZZ} = \frac{(N_C^f)^2}{64\pi^5} \left(\frac{gm_f}{2M_W} \right)^2 \left(\frac{g}{4\cos\theta_W} \right)^4$. The \mathcal{G} 's and \mathcal{F} 's functions contain Passarino-Veltman functions and also depend on the ratios r_f and r_Z .

2. The decay width for $A^0 \rightarrow Z\gamma$ is given by the following expression:

$$\Gamma(A^0 \rightarrow Z\gamma) = m_A \frac{g_v^{f^2} \kappa_{Z\gamma} r_f}{(1 - r_Z)} \left(g_P^{f^2} m_A^4 (r_Z - 1)^4 C_0(m_Z, 0)^2 + 2g_S^{f^2} \left(m_A^2 (1 - r_Z) (4r_f + r_Z - 1) C_0(m_Z, 0) + 2(\Delta B_0(m_A, m_Z, 0) - 1) r_Z + 2 \right)^2 \right),$$

$$\text{where } \kappa_{Z\gamma} = \frac{(N_C^f)^2}{64\pi^5} \left(\frac{gm_f}{2m_W} \right)^2 \left(\frac{g}{4\cos\theta_W} \right)^2 \left(e|Q_f| \right)^2.$$

3. The decay width for $A^0 \rightarrow \gamma\gamma$ is given by

$$\Gamma(A^0 \rightarrow \gamma\gamma) = m_A r_f \kappa_{\gamma\gamma} \left(I_f^2 g_P^{f^2} + 2g_S^{f^2} (I_f (4r_f - 1) + 2)^2 \right), \quad (12)$$

$$\text{where } I_f = C_0(0, 0) m_A^2 \text{ and } \kappa_{\gamma\gamma} = \frac{(N_C^f)^2}{128\pi^5} \left(\frac{gm_f}{2m_W} \right)^2 \left(e|Q_f| \right)^4$$

IV. RESULTS AND LHC ANALYSIS

The recent LHC results have shown that the observed Higgs boson properties are very similar to the ones predicted by the SM, although some small deviations have persisted, which would suggest the possible presence of new physics effects. Within the 2HDM, those new effects depend on the mixing angles and the scale μ_{12} , and thus in order to get small deviations with respect to SM, we shall choose the following set of parameters,

$$\mu_{12} = 200 \text{ GeV} \sim v, \quad (13)$$

$$\beta - \alpha = \frac{\pi}{2} + \delta, \quad (14)$$

where v is the electroweak scale, and δ is small. Thus, the above scenario remains close to the SM limit.

A. Numerical results for the branching ratios

For the 2HDM of type II, the mass of the charged Higgs is constrained to be above a value of order 350 GeV. For the 2HDM of type-I the charged Higgs mass is less constrained, and it is possible to have a light charged Higgs, and similarly for the 2HDM of type III [30]. However, in order to explore a common scenario for 2HDM of type I,II and III, we shall consider $m_{H^\pm} = 350$ GeV.

In Fig. 2 we show the results for the branching ratio of the pseudoscalar boson A^0 for the 2HDM of type I and II. For THDM-I (see plot **a** (left) in Fig. 2), we can see that whenever the channels Zh, ZH, WH^\pm are kinematically allowed, they become dominant, and the rest of the modes are suppressed, except for the decay into top quark pair, which can dominate in a small window around 350-400 GeV. The mode $A^0 \rightarrow \gamma\gamma$ has a BR of order 10^{-3} in the best case, for $m_A \simeq 200$ GeV, while the BR's for the modes γZ and ZZ are suppressed with respect to $\gamma\gamma$ by one and two orders of magnitude, respectively. However, when the mass of A is not enough to produce the final states Zh, ZH, WH^\pm , the modes $b\bar{b}$, gg or even $\tau\tau$ could become relevant.

For 2HDM-II (see plot **b** (right) in Fig. 2) the modes $b\bar{b}$ and ZH are the dominant channels, while the decay into gluons gets more suppressed. In this case the mode $A^0 \rightarrow \gamma\gamma$ has a BR of order 2×10^{-5} , at most, for $m_A \simeq 350$ GeV, while the BR for the modes γZ and ZZ is about one order of magnitude smaller.

In Fig. 3 we present the results for the BR corresponding to the 2HDM of type III, in the CP -Conserving limit. But even in this case the Yukawa couplings are different with respect to the models with Z_2 -symmetry, as it was shown in table I. In plot **a** (left) we considered $\chi_{ff} = -1$, and for a light boson A^0 the most important channel is $A^0 \rightarrow b\bar{b}$. In this case we find $\text{BR}(A^0 \rightarrow \gamma\gamma) \simeq 2 \times 10^{-4}$ for $m_A \simeq 350$ GeV. For the same mass, the modes $A^0 \rightarrow \gamma Z, ZZ$ have BR's of order 10^{-5} . On the other hand, in plot **b** (right), we fix $\chi_{ff} = 1$, and this choice significantly affects the channels $A^0 \rightarrow b\bar{b}$ and $A^0 \rightarrow \tau\tau$, reducing them even by about one order of magnitude. For this reason, the $\text{BR}(A^0 \rightarrow gg)$ becomes the dominant one for low masses. But now the mode $\gamma\gamma$ gets enhanced, and can reach BR

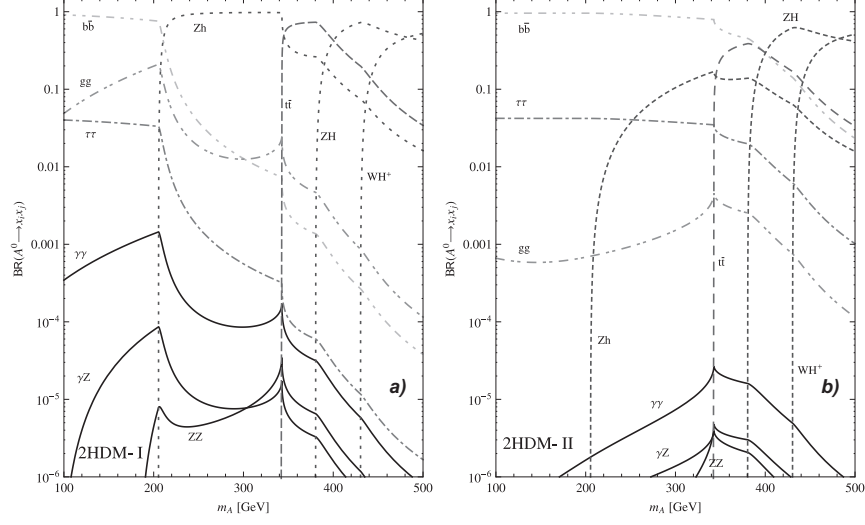


FIG. 2. Branching ratios for the pseudoscalar A^0 in 2HDM of type I and II. The parameter are: $m_H = 300$ GeV, $m_h = 125$ GeV, $m_{H^\pm}^\pm = 350$ GeV, $\tan \beta = 5$ and $\delta = 0.1$.

of order 6×10^{-3} . The modes γZ and ZZ are also enhanced, but have BR at most of order 3×10^{-4} .

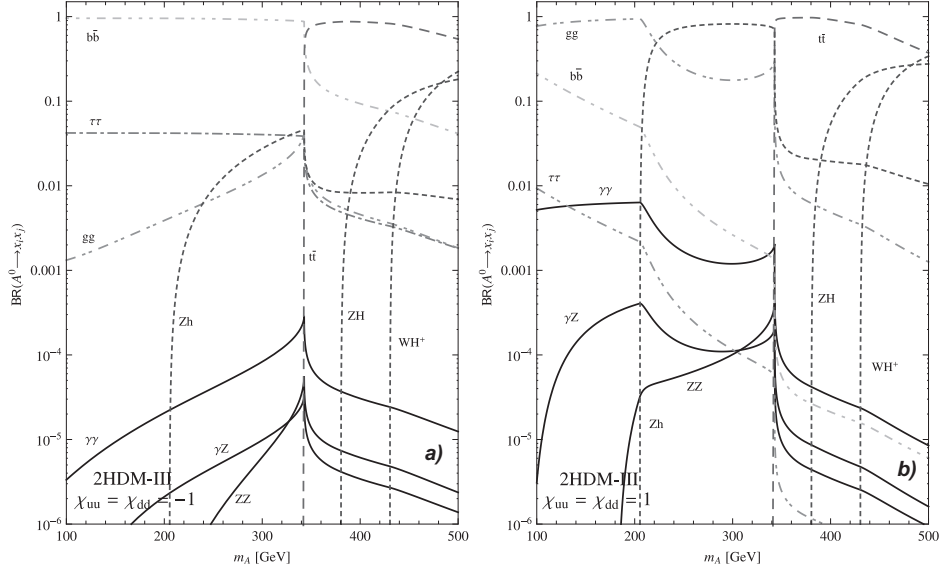


FIG. 3. Branching ratios for the pseudoscalar A^0 within 2HDM of type III in the CP -conserving limit. The parameter are chosen as: $m_H = 300$ GeV, $m_h = 125$ GeV, $m_{H^\pm}^\pm = 350$ GeV, $\tan \beta = 5$ and $\delta = 0.1$.

In order to understand the dependence of the branching ratios on the parameters of the model, we present in Fig. 4, the total decay width for the pseudoscalar A^0 state, as

a function of $\tan\beta$, for the models of type I, II and III. In plot a) (left) we have chosen a value of A mass slightly above the threshold for the decay into top quark pair, namely $m_A = 355 > 2m_t$, while for plot b) (right) we have fixed $m_A = 200$ GeV. We can see that for 2HDM-I, the total width decreases with $\tan\beta$, because all fermionic couplings go like $\cot\beta$, and this is so for both mass values of A . For 2HDM-II one notice that for $m_A = 200$ GeV, the total width just grows with $\tan\beta$, a situation that reflects the fact that the total width is dominated by the decay $A \rightarrow b\bar{b}$, while for $m_A = 200$ GeV the total width starts decreasing for low $\tan\beta$ ($\simeq 1 - 4$), but then increases with $\tan\beta > 4$. In this case, such behavior reflects the interplay between the decays $A \rightarrow b\bar{b}$ and $A \rightarrow t\bar{t}$. In the case of the 2HDM of type III, we observe a behavior of the total decay width that grows with $\tan\beta$, but with a more milder dependence.

In Ref. 5, we show the $\tan\beta$ dependence of the BR into gamma pairs, as well as the corresponding partial width. When one chooses a value $m_A = 355$ GeV, we can see that for 2HDM-I and 2HDM-II, the decrease of $BR(A \rightarrow \gamma\gamma)$ with $\tan\beta$, just reflects the corresponding behavior of $\Gamma(A \rightarrow \gamma\gamma)$; while for 2HDM-III the dependence of $BR(A \rightarrow \gamma\gamma)$ on $\tan\beta$ comes from a combined effect of the $\tan\beta$ dependence of the partial and total widths. On the other hand, when we choose $m_A = 200$ GeV, within 2HDM-I $BR(A \rightarrow \gamma\gamma)$ remains constant, despite the fact that $\Gamma(A \rightarrow \gamma\gamma)$ decreases with $\tan\beta$, but in this case the total width shows a similar suppression, which explains the constant value of $BR(A \rightarrow \gamma\gamma)$. Similar behavior is obtained for the modes $A \rightarrow Z\gamma$ and $A \rightarrow ZZ$. Overall, one can see from these plots, that the 2HDM-II present the most sensitive results, showing a variation of about four orders of magnitude for $\gamma\gamma$ and γZ , and more than four orders of magnitude for ZZ . In contrast, the 2HDM-III with $\chi_{ff} = 1$ is less sensitive to $\tan\beta$; this scenario presents small variations (of order unity) for all cases.

In Fig.6 we show the branching ratio for $A \rightarrow Z\gamma$, and the corresponding partial decay width, as function of $\tan\beta$. For $m_A = 355$ GeV, the BR for this mode decrease with $\tan\beta$, within 2HDM-I, II and III (with $\chi = -1$), while within 2HDM-III with $\chi = 1$, the BR remains almost constant. On the other hand, when one chooses $m_A = 200$ GeV, we find that the BR decreases with $\tan\beta$, within 2HDM-II and 2HDM-III (with $\chi = -1$), while within 2HDM-I and 2HDM-III (with $\chi = 1$), the BR remains almost constant.

On the other hand, we show in Fig. 7 the $\tan\beta$ dependence of $BR(A \rightarrow ZZ)$ and $\Gamma(A \rightarrow ZZ)$. When $m_A = 355$ GeV the branching ratios decreases as function of $\tan\beta$

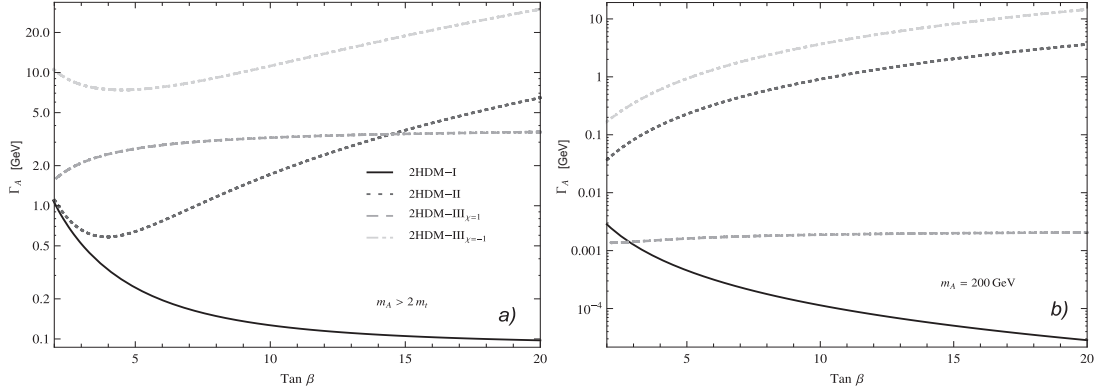


FIG. 4. Behavior of total width Γ_A as a function of $\tan \beta$. The parameter are choosen as: $m_H = 300$ GeV, $m_h = 125$ GeV, $m_{H^\pm} = 350$ GeV and $\delta = 0.1$. The assignment of line codes appears in the plot **a**, where we fixed $m_A = 355$ GeV ($> 2m_t$), while in plot **b** we take $m_A = 200$ GeV.

within 2HDM-I, II and 2HDM-III (with $\chi = -1$), while within 2HDM-III with $\chi = 1$, the BR remains almost constant. When $m_A = 200$ GeV the BR decreases with $\tan \beta$ within 2HDM-II and III (with $\chi = -1$); while within 2HDM-I and 2HDM-III (with $\chi = 1$), the BR remains almost constant. We also notice that the $\Gamma(A \rightarrow ZZ)$ have a sharp decrease within 2HDM-II for $\tan \beta \sim 5$ and within 2HDM-III (with $\chi = -1$) for $\tan \beta \sim 12$, respectively.

B. Constraints from LHC search for heavy Higgs bosons

The first constraint that any extended model should fulfill nowadays is the occurrence of a light Higgs state with a mass near $m_{h^0} \simeq 125$ GeV. After considering the results, including statistical and systematic uncertainties reported by ATLAS and CMS [1, 2], we consider a central value for m_{h^0} of 125 GeV and an uncertainty of ± 3 GeV; i.e., we accept a value of m_{h^0} in our numerical analysis if it lies within the range [122-128 GeV]. Next, we also need to fullfil the constraints coming from the comparison with the SM-like Higgs signal observed at the LHC.

Thus, in order to compare the signal rate observed for the SM-like Higgs signals, with mass $m_{h^0} \simeq 125$ GeV, arising within the 2HDM model, one can describe the signal strength by the following ratios:

$$R_{XX} = \frac{\sigma(gg \rightarrow h^0)}{\sigma(gg \rightarrow \phi_{sm})} \frac{BR(h^0 \rightarrow XX)}{BR(\phi_{sm} \rightarrow XX)} \quad (15)$$

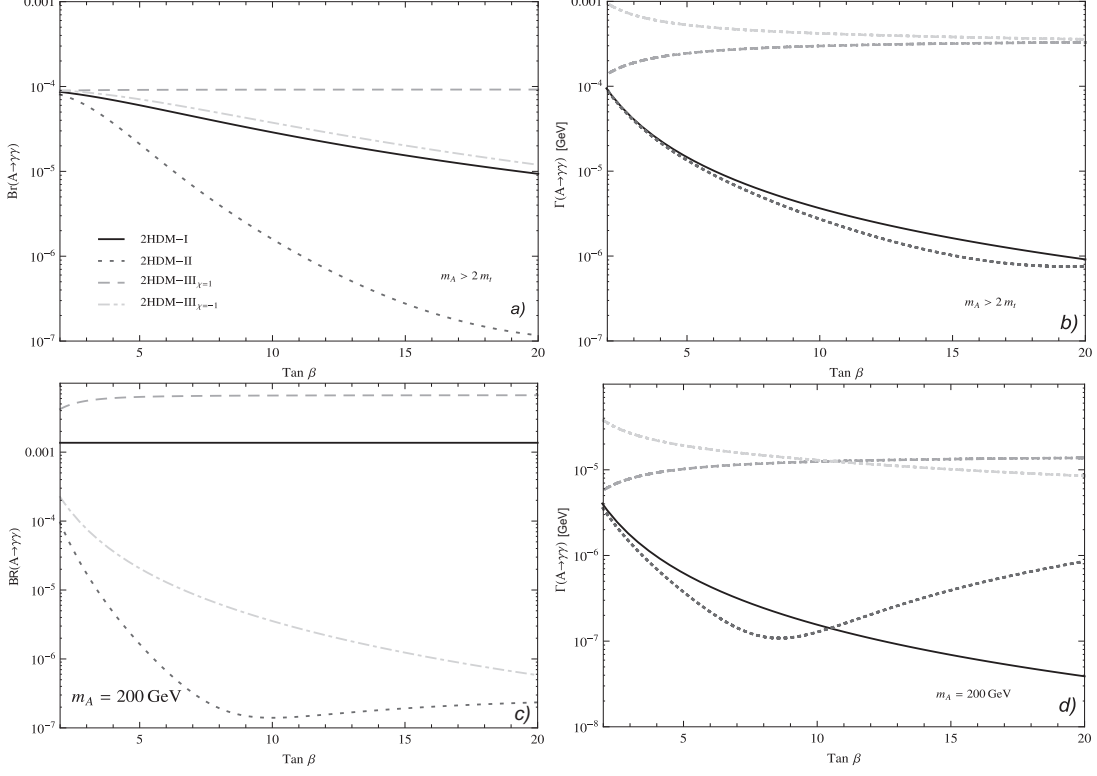


FIG. 5. Behavior of $BR(A^0 \rightarrow \gamma\gamma)$ and $\Gamma(A^0 \rightarrow \gamma\gamma)$ as a function of $\tan\beta$. The parameter are chosen as $m_H = 300$ GeV, $m_h = 125$ GeV, $m_{H^\pm} = 350$ GeV and $\delta = 0.1$. The assignment of line codes appears in the plot **a**.

for $X = \gamma, Z$.

Within the so-called narrow-width approximation, we can write the above expression for R_{XX} as follows:

$$R_{XX} = \frac{\Gamma(h^0 \rightarrow gg)}{\Gamma(\phi_{sm} \rightarrow gg)} \frac{BR(h^0 \rightarrow XX)}{BR(\phi_{sm} \rightarrow XX)} \quad (16)$$

According to the CMS Collaboration the signal strength for the $\gamma\gamma$ channel is $R_{\gamma\gamma} = 0.78^{+0.28}_{-0.26}$, while for the ZZ channel it is $R_{ZZ} = 0.9^{+0.30}_{-0.24}$. Thus, the light Higgs boson of the 2HDM, should satisfy the above conditions, which is achieved in our scenarios because the properties of the light Higgs boson were chosen to be very similar to the SM.

On the other hand, the LHC has also presented limits on the mass of a heavier Higgs boson, which could be used in order to obtain some constraints on the mass of the pseudoscalar state A . We are aware that the pseudoscalar nature of A will affect the distributions of the particles appearing in the final states, and strictly speaking those bounds that searched for the SM-Higgs can not be applied to the pseudoscalar. However, we shall assume that those

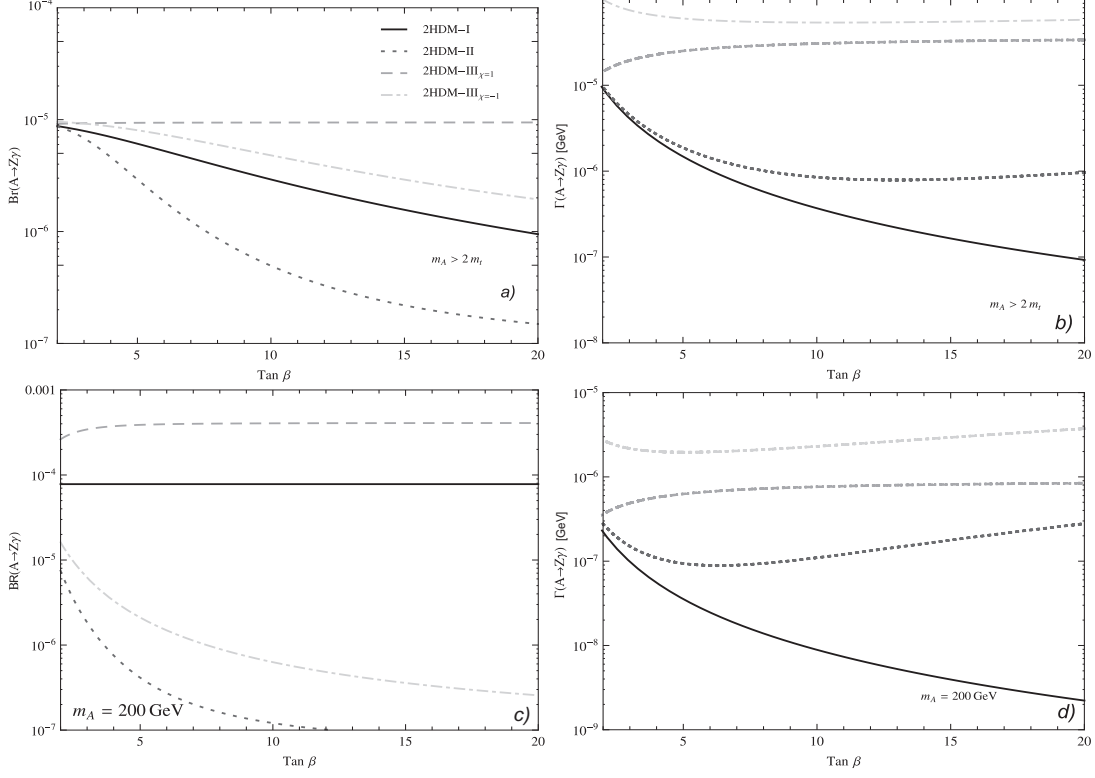


FIG. 6. Behavior of $\text{BR}(A^0 \rightarrow Z\gamma)$ and $\Gamma(A^0 \rightarrow Z\gamma)$ as a function of $\tan\beta$. The parameter are chosen as: $m_H = 300$ GeV, $m_h = 125$ GeV, $m_{H^\pm} = 350$ GeV and $\delta = 0.1$. The assignment of line codes appears in plot **a**.

differences are small enough, at least in order to obtain an estimate for the constraints on the corresponding mass.

For this purpose, we evaluate the ratio

$$R_{XX} = \frac{\sigma(gg \rightarrow A^0)\text{BR}(A^0 \rightarrow XX)}{\sigma(gg \rightarrow \phi_{sm})\text{BR}(\phi_{sm} \rightarrow XX)} \quad (17)$$

$$= \frac{\Gamma(A^0 \rightarrow gg)\text{BR}(A^0 \rightarrow XX)}{\Gamma(\phi_{sm} \rightarrow gg)\text{BR}(\phi_{sm} \rightarrow XX)} \quad (18)$$

at a mass value $m_{\phi_{sm}} = m_A$, which we vary over the range $180 < m_A < 360$ GeV, in order to stay below the threshold for the decay into top pair, which becomes dominant then. The results are shown in the following Fig. 8, which shows the values of R_{ZZ} and $R_{\gamma\gamma}$ vs m_A for 2HDM-I, II and III. We have included the CMS exclusion contour for each channel (ZZ and $\gamma\gamma$), and whenever the predictions from the models fall above these lines, such scenarios would be excluded.

From the left figure, we can see that all models satisfy the constraints imposed by the

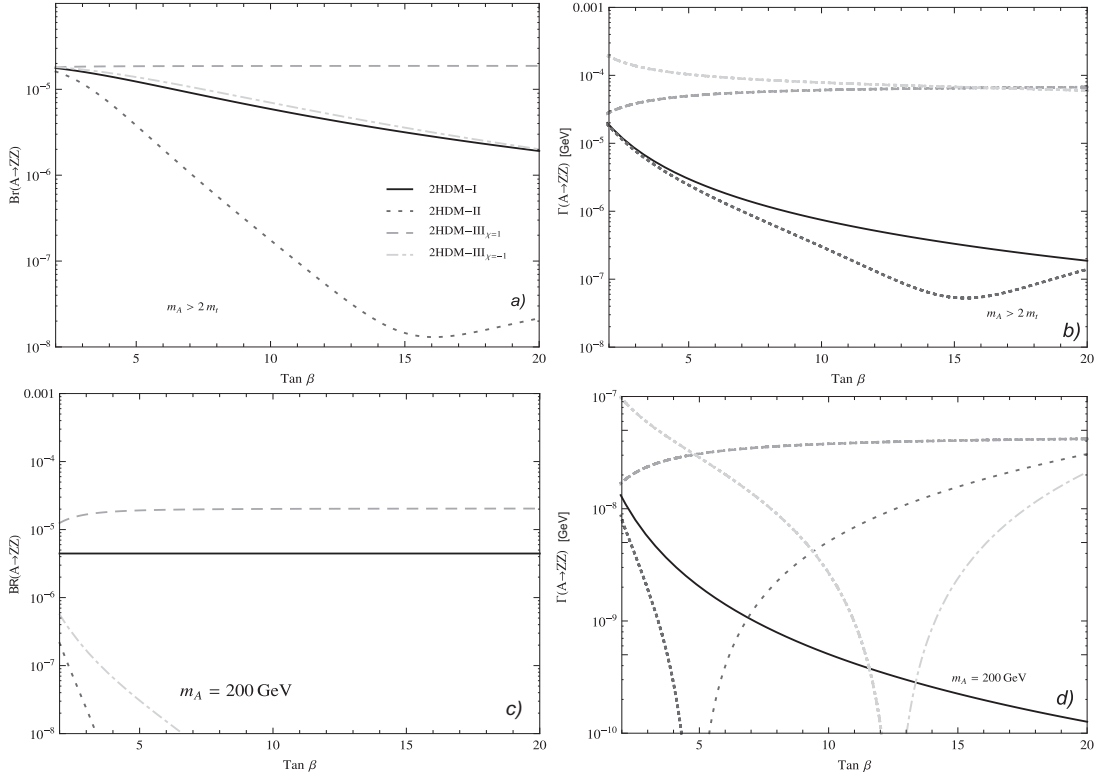


FIG. 7. Behavior of $\text{BR}(A^0 \rightarrow ZZ)$ and $\Gamma(A^0 \rightarrow ZZ)$ as a function of $\tan \beta$. The parameter are chosen as: $m_H = 300 \text{ GeV}$, $m_h = 125 \text{ GeV}$, $m_{H^\pm} = 350 \text{ GeV}$ and $\delta = 0.1$. The assignment of line codes appears in plot **a**.

heavy Higgs search in the ZZ channel. On the other hand, we can see from the right figure, that the values of $R_{\gamma\gamma}$ bounded at LHC, could exclude the mass range $100 < m_A < 160 \text{ GeV}$ for the 2HDM of type III for the choice $\chi = 1$. The 2HDM of type II satisfy this constraint for the mass range $180 < m_A < 360 \text{ GeV}$, while 2HDM-I and 2HDM-III (with $\chi = -1$) seem to be excluded only in the mass range $138 < m_A < 144 \text{ GeV}$. These are promising results which deserve to be looked at in more detail by the experimental LHC Collaborations.

V. CONCLUSIONS

As it is well known, the general two-Higgs doublet model (2HDM) contains a rich spectrum of neutral and charged Higgs bosons, whose detection at current and future colliders would be a clear signal of new physics. When the Higgs potential is CP conserving, the neutral spectrum includes a pseudoscalar mass eigenstate A^0 . Even in this case, the in-

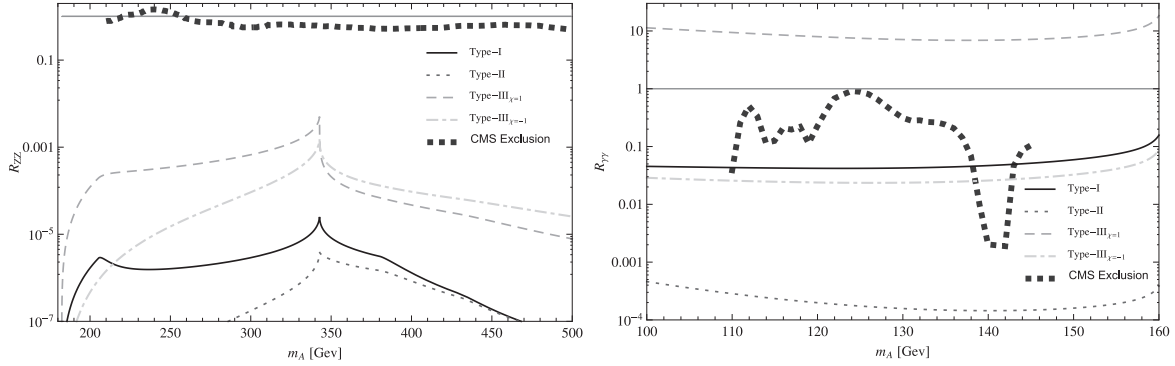


FIG. 8. R_{ZZ} and $R_{\gamma\gamma}$ vs m_A in 2HDM-I-II and III.

interactions of A^0 with fermions could include a CP-violating contribution, arising from a possible non-Hermiticity of the Yukawa matrices. When the Higgs sector is CP conserving, the A^0 boson does not couple to vector bosons at tree level. However the coupling (AVV') is generated at loop level, from fermionic and bosonic loops. The dominant contribution in the low and moderate $\tan\beta$ ($\simeq 1 - 5$), comes from the top quark, while for larger values of $\tan\beta$, the bottom quark contribution becomes relevant.

We have evaluated the generic fermionic contribution to the decays $A^0 \rightarrow ZZ, Z\gamma, \gamma\gamma$, including its scalar and pseudoscalar vertices. Then, we have presented numerical results for the branching ratios. We found that there are regions of parameters where such loop-induced modes could reach significant branching ratios. Current LHC searches for heavy Higgs bosons are used to derive an estimated constraint on the parameters of the models. We find that for 2HDM-II the whole mass range is acceptable, for our choices of parameters, while the 2HDM-III with $\chi = 1$ is excluded in the mass range ($100 < m_A < 160$ GeV). On the other hand, 2HDM-I and 2HDM-III (with $\chi = -1$) seem to be excluded only in the mass range $138 < m_A < 144$ GeV. These scenarios should be further studied at the LHC13 in order to confirm the estimates for exclusion limits presented in this paper.

ACKNOWLEDGMENTS

We acknowledge support from CONACYT-SNI (Mexico), and discussions with J. Montano, who participated in the early stages of this work. We would like to thank M. Wiebusch,

et al. for bringing Ref. [17] to our attention after our paper was submitted to E-prints.

-
- [1] G. Aad *et al.* [ATLAS Collaboration], Phys. Lett. B **716**, 1 (2012) [arXiv:1207.7214 [hep-ex]].
 - [2] S. Chatrchyan *et al.* [CMS Collaboration], Phys. Lett. B **716**, 30 (2012) [arXiv:1207.7235 [hep-ex]].
 - [3] J. Erler, AIP Conf. Proc. **917**, 244 (2007) [hep-ph/0701261].
 - [4] J. F. Gunion, H. E. Haber, G. L. Kane and S. Dawson, Front. Phys. **80**, 1 (2000).
 - [5] G. L. Kane, P. Kumar, D. E. Morrissey and M. Toharia, Phys. Rev. D **75**, 115018 (2007) [hep-ph/0612287].
 - [6] A. Arbey, M. Battaglia, A. Djouadi and F. Mahmoudi, Phys. Lett. B **720**, 153 (2013) [arXiv:1211.4004 [hep-ph]].
 - [7] E. Arganda, J. L. Diaz-Cruz and A. Szyrkman, Phys. Lett. B **722**, 100 (2013) [Phys. Lett. B **722**, 100 (2013)] [arXiv:1301.0708 [hep-ph]].
 - [8] E. Arganda, J. L. Diaz-Cruz and A. Szyrkman, Eur. Phys. J. C **73**, 2384 (2013) [arXiv:1211.0163 [hep-ph]].
 - [9] A. Chakraborty, B. Das, J. L. Diaz-Cruz, D. K. Ghosh, S. Moretti and P. Poulose, arXiv:1301.2745 [hep-ph].
 - [10] S. P. Martin, In *Kane, G.L. (ed.): Perspectives on supersymmetry II* 1-153 [hep-ph/9709356].
 - [11] M. Quiros, hep-ph/0606153.
 - [12] A. Pomarol, CERN Yellow Report CERN-2012-001, 115-151 [arXiv:1202.1391 [hep-ph]].
 - [13] J. L. Diaz-Cruz, JHEP **0305**, 036 (2003) [hep-ph/0207030];
 - [14] G. C. Branco, P. M. Ferreira, L. Lavoura, M. N. Rebelo, M. Sher and J. P. Silva, Phys. Rept. **516**, 1 (2012) [arXiv:1106.0034 [hep-ph]].
 - [15] I. F. Ginzburg and M. Krawczyk, Phys. Rev. D **72**, 115013 (2005) [hep-ph/0408011].
 - [16] A. Mendez and A. Pomarol, Phys. Lett. B **272**, 313 (1991).
 - [17] W. Bernreuther, P. Gonzalez and M. Wiebusch, Eur. Phys. J. C **69**, 31 (2010) [arXiv:1003.5585 [hep-ph]].
 - [18] M. A. Perez, J. J. Toscano and J. Wudka, Phys. Rev. D **52**, 494 (1995) [hep-ph/9506457].
 - [19] J. L. Diaz-Cruz, J. Hernandez-Sanchez and J. J. Toscano, Phys. Lett. B **512**, 339 (2001)

- [hep-ph/0106001].
- [20] T. P. Cheng and M. Sher, Phys. Rev. D **35**, 3484 (1987).
 - [21] J. L. Diaz-Cruz, R. Noriega-Papaqui and A. Rosado, Phys. Rev. D **69**, 095002 (2004) [hep-ph/0401194].
 - [22] W. Altmannshofer, S. Gori and G. D. Kribs, Phys. Rev. D **86**, 115009 (2012) [arXiv:1210.2465 [hep-ph]].
 - [23] N. G. Deshpande and E. Ma, Phys. Rev. D **18**, 2574 (1978).
 - [24] J. L. Diaz-Cruz, R. Noriega-Papaqui and A. Rosado, Phys. Rev. D **71**, 015014 (2005) [hep-ph/0410391].
 - [25] J. L. Diaz-Cruz, A. Diaz-Furlong and J. H. Montes de Oca, arXiv:1010.0950 [hep-ph].
 - [26] M. Arroyo, J. L. Diaz-Cruz, E. Diaz and J. A. Orduz-Ducuara, arXiv:1306.2343 [hep-ph].
 - [27] A. J. Buras, M. V. Carlucci, S. Gori and G. Isidori, JHEP **1010**, 009 (2010) [arXiv:1005.5310 [hep-ph]].
 - [28] A. Crivellin, A. Kokulu and C. Greub, Phys. Rev. D **87**, no. 9, 094031 (2013) [arXiv:1303.5877 [hep-ph]].
 - [29] R. Pittau, JHEP **1211** (2012) 151 [arXiv:1208.5457 [hep-ph]].
 - [30] A. Cordero-Cid, J. Hernandez-Sanchez, C. G. Honorato, S. Moretti, M. A. Perez and A. Rosado, arXiv:1312.5614 [hep-ph]; J. Hernandez-Sanchez, S. Moretti, R. Noriega-Papaqui and A. Rosado, JHEP **1307**, 044 (2013) [arXiv:1212.6818].